

NATIONAL INSTITUTE FOR FUSION SCIENCE

Hybrid Modes in a Square Corrugated Waveguide

K. Ohkubo

(Received - May 25, 2001)

NIFS-702

June 2001

This report was prepared as a preprint of work performed as a collaboration research of the National Institute for Fusion Science (NIFS) of Japan. This document is intended for information only and for future publication in a journal after some rearrangements of its contents.

Inquiries about copyright and reproduction should be addressed to the Research Information Center, National Institute for Fusion Science, Oroshi-cho, Toki-shi, Gifu-ken 509-02 Japan.

RESEARCH REPORT
NIFS Series

Hybrid Modes in a Square Corrugated Waveguide

K. Ohkubo

*National Institute for Fusion Science,
Toki, 509-5292, Japan*

Abstract: By using two scalar eigenfunctions, electric and magnetic fields in the rectangular (or square) corrugated waveguide are analyzed. In a rectangular corrugated waveguide, the boundary conditions on two corrugated and two smooth walls can be satisfied to excite the hybrid mode. In a highly oversized waveguide where the wavelength of dominant mode is close to that in vacuum, two smooth walls can be exchanged with the corrugated walls because the boundary condition at this walls is satisfied approximately. The replacement is possible due to almost no penetration of the electromagnetic fields into the gap of the replaced walls when the direction of main electric field is parallel to the gap of replaced walls. This characteristic enables us to rotate the polarization of the hybrid mode in the oversized square waveguide with all four corrugated walls and is applicable to the remote steering antenna for electron cyclotron heating in the ITER. For a beam injection larger than the critical angle in this antenna, excited higher modes are at a considerably different wavelength from that in vacuum and result in the dissatisfaction of boundary conditions due to millimeter-wave penetration into corrugation gaps in replaced walls.

Keywords: *square corrugated waveguide, polarization, electron cyclotron heating*

1 Introduction

Oversized circular corrugated waveguides have been used in the transmission of high-power millimeter wave for electron cyclotron heating of fusion plasmas [1]. The propagating HE_{11} mode in the waveguide has small attenuation and linear polarization appropriate to polarization control for plasma heating. Meanwhile, except for recurrence characteristics applications, the utilization of rectangular (or square) waveguides with two corrugated walls have received little attention, mainly due to the dissatisfaction of boundary conditions when all the four walls are corrugated [2]. In a weakly oversized waveguide with all the walls corrugated, difficulties in measuring the propagation and an attenuation in 10 to 50 dB was reported in the centimeter wave range [3]. Recently, in a highly oversized square corrugated waveguide which is being developed as an alternative launcher for the ITER [4, 5], loss-free propagation with no change in radiation pattern for rotation of the polarization has been observed for millimeter waves [6]. The purpose of this paper is to explain the two experimental results from weakly and strongly oversized corrugated waveguides and to discuss their utilization as an alternative antenna for the ITER electron cyclotron heating and current drive. Here, an analysis of the electric and magnetic fields in the corrugated waveguide by two scalar eigenfunctions

is introduced without using the traditional Hertzian [2, 3] or vector potential analysis [7].

2 Field Structure

The waveguide fields \mathbf{E} and \mathbf{H} of propagating wave with propagation constant $\beta_{[i]}$ and $\beta_{(i)}$ are written as the sum of TE and TM modes with coefficients V and I . The transverse fields $\mathbf{E}_t, \mathbf{H}_t$ and the longitudinal fields E_z, H_z in the waveguide with the size of $a \times b$ are expressed as [8]

$$\begin{aligned} \mathbf{E}_t &= \sum_i V_{[i]}(z) \mathbf{e}_{[i]} + \sum_i V_{(i)}(z) \mathbf{e}_{(i)} \\ \mathbf{H}_t &= \sum_i I_{[i]}(z) \mathbf{h}_{[i]} + \sum_i I_{(i)}(z) \mathbf{h}_{(i)} \\ E_z &= \frac{Z_0}{jk_0} \sum_i I_{(i)}(z) k_{c(i)}^2 \phi_i \\ H_z &= \frac{1}{jk_0 Z_0} \sum_i V_{[i]}(z) k_{c[i]}^2 \psi_i \end{aligned}$$

where the suffixes $[i]$ and (i) represent i -th mode of TE and TM modes and i is a double index of two mode numbers and also $Z_0 = \sqrt{\mu_0/\epsilon_0}$ and $k_0 = \omega/c$. The TE mode functions $\mathbf{e}_{[i]}, \mathbf{h}_{[i]}$ and the TM mode functions $\mathbf{e}_{(i)}, \mathbf{h}_{(i)}$ possess the property of orthogonality. By solving the wave equations on ψ_i and

ϕ_i

$$\nabla_t^2 \psi_i + k_{c[i]}^2 \psi_i = 0$$

$$\nabla_t^2 \phi_i + k_{c(i)}^2 \phi_i = 0$$

with $k_{c[i]}^2 = k_0^2 - \beta_{[i]}^2$ and $k_{c(i)}^2 = k_0^2 - \beta_{(i)}^2$, and by substituting ψ_i and ϕ_i in

$$\mathbf{e}_{[i]} = \mathbf{a}_z \times \nabla_t \psi_i, \quad \mathbf{h}_{[i]} = \mathbf{a}_z \times \mathbf{e}_{[i]}$$

and

$$\mathbf{e}_{(i)} = -\nabla_t \phi_i, \quad \mathbf{h}_{(i)} = \mathbf{a}_z \times \mathbf{e}_{(i)}$$

mode functions are obtained, where \mathbf{a}_σ ($\sigma = x, y, z$) is the unit vector and $\nabla_t = \nabla - \mathbf{a}_z \partial / \partial z$. Amplitude ratios of V to I are given by

$$V_{[i]} / I_{[i]} = Z_0 k_0 / \beta_{[i]}$$

$$V_{(i)} / I_{(i)} = Z_0 \beta_{(i)} / k_0$$

for TE and TM modes, respectively. The electric and magnetic fields in the rectangular waveguide as shown in Figure 1 are thus obtained by

$$\mathbf{E}_{[i]} = -\left(\frac{\partial \psi_i}{\partial y} \mathbf{a}_x - \frac{\partial \psi_i}{\partial x} \mathbf{a}_y\right) V_{[i]}$$

$$\mathbf{H}_{[i]} = -\left(\frac{\partial \psi_i}{\partial x} \mathbf{a}_x + \frac{\partial \psi_i}{\partial y} \mathbf{a}_y + \frac{j k_{c[i]}^2 \psi_i}{\beta_{[i]}} \mathbf{a}_z\right) \frac{\beta_{[i]}}{Z_0 k_0} V_{[i]}$$

for the TE mode and

$$\mathbf{E}_{(i)} = -\left(\frac{\partial \phi_i}{\partial x} \mathbf{a}_x + \frac{\partial \phi_i}{\partial y} \mathbf{a}_y + \frac{j k_{c(i)}^2 \phi_i}{\beta_{(i)}} \mathbf{a}_z\right) V_{(i)}$$

$$\mathbf{H}_{(i)} = \left(\frac{\partial \phi_i}{\partial y} \mathbf{a}_x - \frac{\partial \phi_i}{\partial x} \mathbf{a}_y\right) \frac{k_0}{Z_0 \beta_{(i)}} V_{(i)}.$$

for the TM mode.

To discuss the electric and magnetic fields of hybrid mode, we define the mode amplitude ratio given by

$$V_{[i]} / V_{(i)} = d_i.$$

By normalizing the power flow $P_{(i)}$ of the TM mode

$$P_{(i)} = \Re(V_{(i)} I_{(i)}^*) = \frac{k_0 |V_{(i)}|^2}{Z_0 \beta_{(i)}} = 1,$$

the mode amplitude

$$V_{(i)} = -\sqrt{R_{(i)} Z_0}$$

is obtained, where $R_{(i)} = \beta_{(i)} / k_0$.

The propagation constants of the TE and TM modes have the same value for $[i] = (i)$ except for the dominant mode. The propagating constant $\beta_{\{i\}}$ of the hybrid mode is calculated by solving the wave equation on the hybrid mode. We replace $\beta_{[i]}$ and $\beta_{(i)}$ with $\beta_{\{i\}}$. The cutoff wavenumbers $k_{c[i]}$ and $k_{c(i)}$ which are derived from $\beta_{[i]}$ and $\beta_{(i)}$ also can be written as $k_{c\{i\}}$. By the same procedure, $R_{[i]}$ and $R_{(i)}$ are exchanged by $R_{\{i\}}$. Here the suffix $\{i\}$ represents the i -th hybrid mode. Thus, the electric and magnetic fields of i -hybrid mode as the sum of TE and TM modes are written by

$$\begin{aligned} \mathbf{E}_i &= \sqrt{R_{\{i\}} Z_0} \left[\left(\frac{\partial \phi_i}{\partial x} + d_i \frac{\partial \psi_i}{\partial y} \right) \mathbf{a}_x + \left(\frac{\partial \phi_i}{\partial y} - d_i \frac{\partial \psi_i}{\partial x} \right) \mathbf{a}_y + j \frac{k_{c\{i\}}^2 \phi_i}{k_0 R_{\{i\}}} \mathbf{a}_z \right] \\ \mathbf{H}_i &= \frac{1}{\sqrt{R_{\{i\}} Z_0}} \left[-\left(\frac{\partial \phi_i}{\partial y} - d_i R_{\{i\}}^2 \frac{\partial \psi_i}{\partial x} \right) \mathbf{a}_x + \left(\frac{\partial \phi_i}{\partial x} + d_i R_{\{i\}}^2 \frac{\partial \psi_i}{\partial y} \right) \mathbf{a}_y + j \frac{k_{c\{i\}}^2 d_i R_{\{i\}} \psi_i}{k_0} \mathbf{a}_z \right]. \end{aligned}$$

These results are consistent with the electromagnetic field acquired for the hybrid mode in the circular corrugated waveguide by co-ordinate inversion [10]. It is confirmed by direct substitution that \mathbf{E}_i and \mathbf{H}_i satisfy the Maxwell equation such that $\text{div}_{\epsilon_0} \mathbf{E}_i = 0$, $\text{div}_{\mu_0} \mathbf{H}_i = 0$, $\text{rot} \mathbf{E}_i = -\partial \mu_0 \mathbf{H}_i / \partial t$, and $\text{rot} \mathbf{H}_i = \partial \epsilon_0 \mathbf{E}_i / \partial t$. Especially, the fields \mathbf{E}_i and \mathbf{H}_i for TE or TM modes are calculated by substituting ($\phi_i = 0$, $d_i = 1/R_{[i]}$) or ($\psi_i = 0$, $d_i = 0$). The cutoff wavenumber $k_{c\{i\}}$ of hybrid mode is obtained from the fact that \mathbf{E}_i (or \mathbf{H}_i) satisfies the wave equation

$$\nabla_t^2 \mathbf{E}_i + k_{c\{i\}}^2 \mathbf{E}_i = 0,$$

where $k_{c\{i\}}^2 = k_0^2 - \beta_{\{i\}}^2$, $R_{\{i\}} = \beta_{\{i\}} / k_0$ is calculated straightforwardly.

When

$$\psi_i = N_i \begin{pmatrix} \sin k_x x \\ \cos k_x x \end{pmatrix} \begin{pmatrix} \sin k_y y \\ \cos k_y y \end{pmatrix}$$

$$\phi_i = N_i \begin{pmatrix} \sin k_x x \\ \cos k_x x \end{pmatrix} \begin{pmatrix} \sin k_y y \\ \cos k_y y \end{pmatrix}$$

are adopted as scalar eigenfunctions, where a sinusoidal function is chosen from the parenthesis, these satisfy the wave equations

$$\nabla_t^2 \psi_i + k_{c\{i\}}^2 \psi_i = -(k_x^2 + k_y^2) \psi_i + k_{c\{i\}}^2 \psi_i = 0$$

$$\nabla_t^2 \phi_i + k_{c\{i\}}^2 \phi_i = -(k_x^2 + k_y^2) \phi_i + k_{c\{i\}}^2 \phi_i = 0.$$

We have $k_{c\{i\}}^2 = k_x^2 + k_y^2$, where k_x and k_y are the separation constants which are introduced for solving

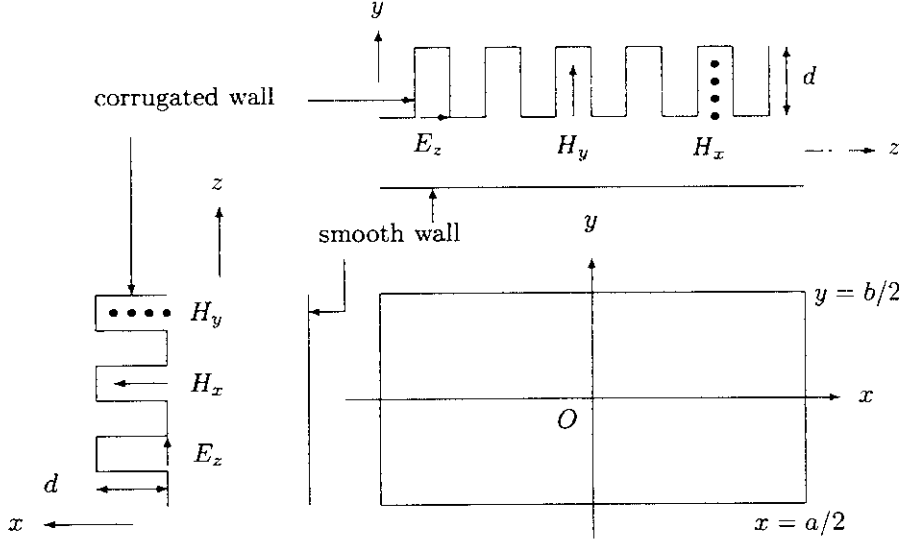


Figure 1: Rectangular waveguide with impedance walls.

the above equations. The origin of the co-ordinates system is located at the center of the waveguide cross-section. In an estimation of \mathbf{E}_i and \mathbf{H}_i by ψ_i and ϕ_i , there exist 16 cases due to four combinations for ψ_i and ϕ_i . In the x - (y -) component of \mathbf{E}_i and in the y - (x -) component of \mathbf{H}_i , $\partial\phi_i/\partial x$ and $\partial\psi_i/\partial y$ ($\partial\phi_i/\partial y$ and $\partial\psi_i/\partial x$) must have the same functional form along the waveguide wall on which boundary condition is evaluated. As a result, the following four cases are valid, *i.e.*

(A) $\psi_i = N_i \sin k_x x \cos k_y y$ and $\phi_i = N_i \cos k_x x \sin k_y y$

(B) $\psi_i = N_i \cos k_x x \sin k_y y$ and $\phi_i = N_i \sin k_x x \cos k_y y$

(C) $\psi_i = N_i \sin k_x x \sin k_y y$ and $\phi_i = N_i \cos k_x x \cos k_y y$

(D) $\psi_i = N_i \cos k_x x \cos k_y y$ and $\phi_i = N_i \sin k_x x \sin k_y y$

The surface impedances appropriate for the rectangular waveguide with smooth or corrugated walls [2] are

$$Z_{ta} = \pm \frac{E_y}{H_z} \Big|_{x=\pm a/2}, \quad Z_{la} = \mp \frac{E_z}{H_y} \Big|_{x=\pm a/2}$$

$$Z_{tb} = \mp \frac{E_x}{H_z} \Big|_{y=\pm b/2}, \quad Z_{lb} = \pm \frac{E_z}{H_x} \Big|_{y=\pm b/2}.$$

The suffixes t and l are related with the transverse and longitudinal directions, respectively. A waveguide wall of two different types can be fabricated such as an isotropic wall matched for $Z_{ta} = Z_{la}$ or $Z_{tb} = Z_{lb}$ and an anisotropic wall matched for

$Z_{ta} \neq Z_{la}$ or $Z_{tb} \neq Z_{lb}$. The anisotropic impedance surface is prepared with a corrugated wall which has the depth d , the width W and the pitch P . In a rectangular waveguide with all four corrugated walls and with small height such as $b < \lambda_0/2$ for centimeter wave range, wave propagation in the slot of side walls at $x = \pm a/2$ is in the cutoff, where $\lambda_0 = 2\pi/k_0$. Its isotropic surface impedance with hyperbolic function form was derived on the corrugated walls at $x = \pm a/2$ [7].

Whilst, in the highly oversized waveguide, the corrugated walls at $x = \pm a/2$ or $y = \pm b/2$ look like a surface with an anisotropic impedance:

$$Z_{ta} = 0, \quad Z_{la} = Z_{coa}$$

or

$$Z_{tb} = 0, \quad Z_{lb} = Z_{cob},$$

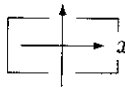
where

$$Z_{coa} = \frac{jWZ_0}{P} \frac{\tan(k_0 d \sqrt{1 - (n\lambda_0/2b)^2})}{\sqrt{1 - (n\lambda_0/2b)^2}}$$

$$Z_{cob} = \frac{jWZ_0}{P} \frac{\tan(k_0 d \sqrt{1 - (m\lambda_0/2a)^2})}{\sqrt{1 - (m\lambda_0/2a)^2}}.$$

Here, m, n are the mode number of the TE_{m0} and TE_{n0} modes excited in the gap and $\lambda_0 = 2\pi/k_0$. For a smooth wall, the surface impedances $Z_{la} = 0$ and $Z_{lb} = 0$ are obtained by $d = 0$. In the following we discuss four cases of (A) to (D) in order. Hereafter, solutions with pure imaginary k_x and k_y for surface wave are not discussed from the viewpoint of real use.

Table 1: Possible wall-shape of the rectangular waveguide in the case of (A). The upper figure in the box shows the exact result and the lower one the alternative shape with the highly oversized approximation ($R_{\{i\}}^2 \simeq 1$). The absence of a figure indicates that boundary condition at $x = \pm a/2$ and/or $y = \pm b/2$ is not satisfied. The arrows show the main electric field.

<div style="display: flex; align-items: center;"> <div style="margin-right: 10px;">waveguide</div>  </div>		$m_p (\neq 0)$					
		$d_i = -k_x/k_y$ $E_y, H_x \propto \cos k_x x \cos k_y y$ $E_x = 0, H_y \simeq 0$		$d_i = k_y/k_x$ $E_x, H_y \propto \sin k_x x \sin k_y y$ $E_y = 0, H_x \simeq 0$			
		odd	even	odd	even	odd	even
n_p ($\neq 0$)	odd						
	even						

Case (A)

With $k_x \neq 0$ and $k_y \neq 0$, the electric and magnetic fields are written by

$$E_x = -N_i \sqrt{R_{\{i\}}} Z_0 (k_x + k_y d_i) \sin k_x x \sin k_y y$$

$$E_y = N_i \sqrt{R_{\{i\}}} Z_0 (k_y - k_x d_i) \cos k_x x \cos k_y y$$

$$E_z = N_i \sqrt{R_{\{i\}}} Z_0 \frac{j k_{c\{i\}}^2}{k_0 R_{\{i\}}} \cos k_x x \sin k_y y$$

$$H_x = -\frac{N_i}{\sqrt{R_{\{i\}}} Z_0} (k_y - k_x d_i R_{\{i\}}^2) \cos k_x x \cos k_y y$$

$$H_y = -\frac{N_i}{\sqrt{R_{\{i\}}} Z_0} (k_x + k_y d_i R_{\{i\}}^2) \sin k_x x \sin k_y y$$

$$H_z = \frac{N_i}{\sqrt{R_{\{i\}}} Z_0} \frac{j k_{c\{i\}}^2 d_i R_{\{i\}}}{k_0} \sin k_x x \cos k_y y.$$

It is noted that E_z and H_z are very small such that $E_z/E_x = O(1/k_0 a)$, $E_z/E_y = O(1/k_0 a)$, $H_z/H_x = O(1/k_0 a)$ and $H_z/H_y = O(1/k_0 a)$. For a highly oversized waveguide with $k_0 a \gg 1$, the propagating wave becomes an almost TEM-like mode. From the field components, Z_{tb} is expressed as

$$Z_{tb} = -\frac{j k_0 Z_0}{k_{c\{i\}}^2 d_i} (k_x + k_y d_i) \tan \frac{k_y b}{2}.$$

To satisfy $Z_{tb} = 0$, two cases are considered:

(A1) $d_i = -k_x/k_y$ which gives $E_x = 0$,

(A2) $k_y = n_e \pi/b$, with $n_e = 2, 4, 6, \dots$

Case (A1) Since

$$Z_{ta} = -\frac{j k_0 Z_0}{k_x} \cot \frac{k_x a}{2}$$

should be zero, we have to select $k_x = m_o \pi/a$ with an odd number for m_o . Thus, Z_{lb} is expressed as

$$Z_{lb} = -\frac{j k_y Z_0}{k_0} \frac{\tan(k_y b/2)}{1 - (m_o \lambda_0/2a)^2}.$$

The separation constant k_y is determined in terms of $Z_{lb} = Z_{cob}$. A numerical calculation of k_y was previously carried out for the rectangular waveguide with two corrugated and two smooth walls [9]. The separation constant $k_y = n_o \pi/b$ with an odd number n_o gives $Z_{lb} = \infty$ which shows that the walls at $y = \pm b/2$ are anisotropic, while $k_y = n_e \pi/b$ with an even number n_e gives an isotropic $Z_{lb} = 0$ which indicates smooth walls at $y = \pm b/2$. On the walls at $x = \pm a/2$, Z_{la} becomes equal to Z_{ta} :

$$Z_{la} = -\frac{j k_0 Z_0}{k_x} \cot \frac{k_x a}{2} = Z_{ta}.$$

The result shows that walls at $x = \pm a/2$ should be smooth and that $E_x = E_y = E_z = 0$, $H_x = 0$, $H_y \neq 0$ and $H_z \neq 0$ at $x = \pm a/2$ are derived. Since $R_{\{i\}}$

in a sufficiently oversized waveguide is approximately equal to unity. H_y in the waveguide cross-section is negligibly small due to $H_y \propto (k_x + k_y d_i R_{\{i\}}^2)$. Here, only the field H_z remains non-zero with satisfaction of the boundary conditions. Even if the smooth walls at $x = \pm a/2$ are replaced with corrugated ones, the electromagnetic fields are not affected by the existence of the corrugation due to $E_x = E_y = E_z = 0$, $H_x = 0$, $H_y \simeq 0$ and $H_z \neq 0$. That is to say, the walls appear to be a metal boundary at $x = \pm a/2$. As an example on the finite H_z , it is well-known that the electric (magnetic) field on a corrugated grating plate is reflected with phase shift of $\pi(0)$ when the incident electric field of the plane wave with normal incidence is parallel to the groove. The electric field parallel to the groove and the magnetic field perpendicular to the groove on the plate become zero and twice the value, respectively.

Thirty years ago, a rectangular waveguide with impedance walls was discussed from the viewpoint of low attenuation [2]. It is shown that completely independent choices of impedances cannot be made and that

$$Z_{la}(Z_{tb} - Z_{lb}) + Z_{lb}Z_{la} = 0$$

must be realized. The rectangular waveguide with all four corrugated walls fails to satisfy the above impedance relation due to $Z_{ta} = Z_{tb} = 0$, $Z_{la} \neq 0$ and $Z_{lb} \neq 0$. It was pointed out that a modal solution cannot be formulated for this configuration. Although the relation abovementioned is satisfied for (A1), we would claim that smooth walls at $x = \pm a/2$ can be replaced with corrugated walls in the highly oversized waveguide due to almost no penetration of the electric and magnetic fields in the groove and that the propagation of the hybrid mode in the waveguide with all four walls corrugated is possible. However, in the weakly oversized waveguide with $R_{\{i\}}^2 \neq 1$, an exchange with corrugated walls is impossible due to $H_y \neq 0$ which yields the penetration of the fields in the groove and an attenuation in the corrugated section. This is the explanation for why low-loss propagation in the highly oversized square waveguide [6] and strong attenuation in the weakly oversized one [3] with all the corrugated walls was observed.

Case (A2) For the case of (A2) as $k_y = n_e \pi/b$, we have

$$Z_{ta} = -\frac{j k_0 Z_0}{k_{c\{i\}}^2 d_i} (k_y - k_x d_i) \cot \frac{k_x a}{2}$$

at $x = \pm a/2$. There exist two possibilities for $Z_{ta} = 0$:

$$(A2.1) \quad d_i = k_y/k_x \text{ which gives } E_y = 0,$$

$$(A2.2) \quad k_x = m_o \pi/a \text{ with } m_o = 1, 3, 5, \dots$$

As for the case of (A2.1), the impedance Z_{lb} is equal to Z_{tb} :

$$Z_{lb} = -\frac{j k_0 Z_0}{k_y} \tan \frac{k_y b}{2} = Z_{tb}.$$

This result shows that walls at $y = \pm b/2$ have isotropic surface impedance and are smooth due to $Z_{tb} = 0$. The impedance Z_{la} is given by

$$Z_{la} = \frac{j k_x Z_0}{k_0} \frac{\cot(k_x a/2)}{1 - (n_e \lambda_0/2b)^2}.$$

The separation constant k_x is calculated from the condition of $Z_{la} = Z_{coa}$. The value of $k_x = m_e \pi/a$ with an even number m_e gives $Z_{la} = \infty$, which shows corrugated walls at $x = \pm a/2$ with depth of $d = \lambda_0/4$, while $k_x = m_o \pi/a$ with an odd number m_o gives $Z_{la} = 0$ which indicates the smooth wall at $x = \pm a/2$. Here, $E_x = E_y = E_z = 0$, $H_x \neq 0$, $H_y = 0$ and $H_z \neq 0$ at $y = \pm b/2$ are obtained. Since $R_{\{i\}}$ in the sufficiently oversized waveguide is approximately equal to unity, H_x in the waveguide cross-section is negligibly small due to $H_x \propto (-k_y + k_x d_i R_{\{i\}}^2)$. Even if smooth walls at $y = \pm b/2$ are replaced with corrugated ones, electromagnetic fields are hardly affected in the presence of the corrugation as above-mentioned.

Finally, in the case of (A2.2) which corresponds to arbitrary d_i , we have $k_x = m_o \pi/a$ and $k_y = n_e \pi/b$. The normal mode is the mixing of TE and TM modes in the smooth waveguide. All the results are summarized in Table 1. The upper figure in the frame indicates the exact result. The lower one shows the approximate alternative wall for the highly oversized waveguide ($R_{\{i\}}^2 \simeq 1$). Especially, when $d = \lambda_0/4$ or $d = 0$, the cutoff wavenumber is expressed as

$$k_{c\{i\}}^2 = \left(\frac{m_p \pi}{a}\right)^2 + \left(\frac{n_p \pi}{b}\right)^2$$

where p is an odd or an even number. For $m_p \pi/(k_0 a) \ll 1$ and $n_p \pi/(k_0 b) \ll 1$, the propagation constant $\beta_{\{i\}}$ is approximated as

$$\beta_{\{i\}} = k_0 \left[1 - \frac{1}{2} \left(\frac{m_p \lambda_0}{2a} \right)^2 - \frac{1}{2} \left(\frac{n_p \lambda_0}{2b} \right)^2 \right].$$

For $m_p = n_p = 1$, $\lambda_0 = 2$ mm and $a = 40$ mm, we obtain $R_{\{i\}}^2 = (\beta_{\{i\}}/k_0)^2 \simeq 0.9994$ with $i = (1, 1)$.

Case (B)

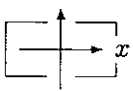

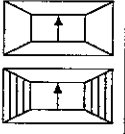
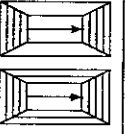
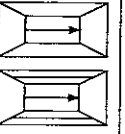
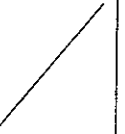
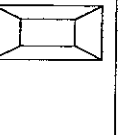

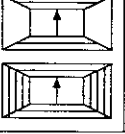

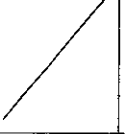
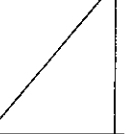
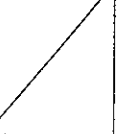
In the case of (B) with $k_x \neq 0$ and $k_y \neq 0$, the electric and magnetic fields are written by

$$E_x = N_i \sqrt{R_{\{i\}}} Z_0 (k_x + k_y d_i) \cos k_x x \cos k_y y$$

$$E_y = -N_i \sqrt{R_{\{i\}}} Z_0 (k_y - k_x d_i) \sin k_x x \sin k_y y$$

$$E_z = N_i \sqrt{R_{\{i\}}} Z_0 \frac{j k_{c\{i\}}^2}{k_0 R_{\{i\}}} \sin k_x x \cos k_y y$$

Table 2: Possible wall-shape of the rectangular waveguide in the case of (B). The upper figure in the box shows the exact result and the lower one the alternative shape with the highly oversized approximation ($R_{\{i\}}^2 \simeq 1$). The absence of a figure indicates that the boundary conditions at $x = \pm a/2$ and/or $y = \pm b/2$ is not satisfied. The arrows show the main electric field.

<div style="display: flex; align-items: center;"> <div style="margin-right: 10px;">waveguide</div>  </div>		$m_p(\neq 0)$					
		$d_i = -k_x/k_y$ $E_y, H_x \propto \sin k_x x \sin k_y y$ $E_x = 0, H_y \simeq 0$		$d_i = k_y/k_x$ $E_x, H_y \propto \cos k_x x \cos k_y y$ $E_y = 0, H_x \simeq 0$			
		odd	even	odd	even	odd	even
n_p ($\neq 0$)	odd						
	even						

$$H_x = \frac{N_i}{\sqrt{R_{\{i\}} Z_0}} (k_y - k_x d_i R_{\{i\}}^2) \sin k_x x \sin k_y y$$

$$H_y = \frac{N_i}{\sqrt{R_{\{i\}} Z_0}} (k_x + k_y d_i R_{\{i\}}^2) \cos k_x x \cos k_y y$$

$$H_z = \frac{N_i}{\sqrt{R_{\{i\}} Z_0}} \frac{j k_{c\{i\}}^2 d_i R_{\{i\}}}{k_0} \cos k_x x \sin k_y y$$

By combination of the various mode number, possible wall shapes are shown in Table 2. With the approximation of $R_{\{i\}}^2 \simeq 1$, $E_x = 0$ and $H_y \simeq 0$ for $d_i = -k_x/k_y$, and also $E_y = 0$ and $H_x \simeq 0$ for $d_i = k_y/k_x$ are obtained. The transverse electric and magnetic fields in $d_i = -k_x/k_y$ ($d_i = k_y/k_x$) are asymmetric (symmetric) with respect to the x - and y -axes. The surface impedances Z_{lb} for $d_i = -k_x/k_y$ and Z_{la} for $d_i = k_y/k_x$ are expressed as

$$Z_{lb} = \frac{j k_y Z_0}{k_0} \frac{\cot(k_y b/2)}{1 - (m_e \lambda_0/2a)^2}$$

with $k_x = m_e \pi/a$ and

$$Z_{la} = -\frac{j k_x Z_0}{k_0} \frac{\tan(k_x a/2)}{1 - (n_o \lambda_0/2b)^2}$$

with $k_y = n_o \pi/b$. The separation constants k_x and k_y in the waveguide with two corrugated walls are determined from solving the equations $Z_{la} = Z_{coa}$ and $Z_{lb} = Z_{cob}$. For the highly oversized waveguide, smooth walls in a specific configuration can

be replaced with corrugated walls with $d = \lambda_0/4$ as in the case of (A). In the highly oversized approximation, the (m_o, n_o) mode with $d_i = k_y/k_x$ is cross-polarized with respect to the (m_o, n_o) mode with $d_i = -k_x/k_y$ in the case of (A). The mode (m_e, n_e) with $d_i = -k_x/k_y$ has the relation of cross-polarization with the (m_e, n_e) mode with $d_i = k_y/k_x$ in the case of (A).

Case (C)

With $k_x \neq 0$ and $k_y \neq 0$, the electric and magnetic fields are written by

$$E_x = -N_i \sqrt{R_{\{i\}} Z_0} (k_x - k_y d_i) \sin k_x x \cos k_y y$$

$$E_y = -N_i \sqrt{R_{\{i\}} Z_0} (k_y + k_x d_i) \cos k_x x \sin k_y y$$

$$E_z = N_i \sqrt{R_{\{i\}} Z_0} \frac{j k_{c\{i\}}^2}{k_0 R_{\{i\}}} \cos k_x x \cos k_y y$$

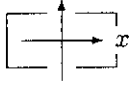
$$H_x = \frac{N_i}{\sqrt{R_{\{i\}} Z_0}} (k_y + k_x d_i R_{\{i\}}^2) \cos k_x x \sin k_y y$$

$$H_y = -\frac{N_i}{\sqrt{R_{\{i\}} Z_0}} (k_x - k_y d_i R_{\{i\}}^2) \sin k_x x \cos k_y y$$

$$H_z = \frac{N_i}{\sqrt{R_{\{i\}} Z_0}} \frac{j k_{c\{i\}}^2 d_i R_{\{i\}}}{k_0} \sin k_x x \sin k_y y$$

It is derived that in the approximation of $R_{\{i\}}^2 \simeq 1$, $E_y = 0$ and $H_x \simeq 0$ for $d_i = -k_y/k_x$ and that

Table 3: Possible wall-shape of the rectangular waveguide in the case of (C). The upper figure in the box shows the exact result and the lower one the alternative shape with the highly oversized approximation ($R_{\{i\}}^2 \simeq 1$). The absence of a figure indicates that the boundary conditions at $x = \pm a/2$ and/or $y = \pm b/2$ is not satisfied. The arrows show the main electric field.

waveguide 		$m_p(\neq 0)$					
		$d_i = -k_y/k_x$ $E_x, H_y \propto \sin k_x x \cos k_y y$ $E_y = 0, H_x \simeq 0$		$d_i = k_x/k_y$ $E_y, H_x \propto \cos k_x x \sin k_y y$ $E_x = 0, H_y \simeq 0$			
		odd	even	odd	even	odd	even
n_p ($\neq 0$)	odd						
	even						

$E_x = 0$ and $H_y \simeq 0$ for $d_i = k_x/k_y$. The transverse electric and magnetic fields change with symmetric and asymmetric dependencies on each axis. Starting from boundary condition $Z_{tb} = 0$ at $x = \pm b/2$ as discussed in the case of (A), the possible mode can be examined. The result satisfying the boundary condition is shown in Table 3.

Case (D)

With $k_x \neq 0$ and $k_y \neq 0$, the electric and magnetic fields are written by

$$\begin{aligned}
 E_x &= N_i \sqrt{R_{\{i\}}} Z_0 (k_x - k_y d_i) \cos k_x x \sin k_y y \\
 E_y &= N_i \sqrt{R_{\{i\}}} Z_0 (k_y + k_x d_i) \sin k_x x \cos k_y y \\
 E_z &= N_i \sqrt{R_{\{i\}}} Z_0 \frac{j k_{c\{i\}}^2}{k_0 R_{\{i\}}} \sin k_x x \sin k_y y \\
 H_x &= -\frac{N_i}{\sqrt{R_{\{i\}}} Z_0} (k_y + k_x d_i R_{\{i\}}^2) \sin k_x x \cos k_y y \\
 H_y &= \frac{N_i}{\sqrt{R_{\{i\}}} Z_0} (k_x - k_y d_i R_{\{i\}}^2) \cos k_x x \sin k_y y \\
 H_z &= \frac{N_i}{\sqrt{R_{\{i\}}} Z_0} \frac{j k_{c\{i\}}^2 d_i R_{\{i\}}}{k_0} \cos k_x x \cos k_y y
 \end{aligned}$$

It is noted that in the highly oversized waveguide such as $R_{\{i\}}^2 \simeq 1$, $E_x = 0$ and $H_y \simeq 0$ for $d_i = k_x/k_y$ and that $E_y = 0$ and $H_x \simeq 0$ for $d_i = -k_y/k_x$. The

results satisfying the boundary condition are shown in Table 4. In the next section, the special cases of $k_x = 0$ or $k_y = 0$ are discussed.

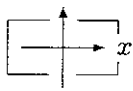



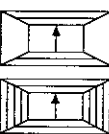


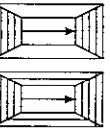
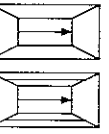

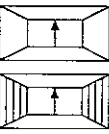

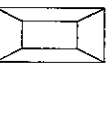
Case $k_x = 0$ or $k_y = 0$

With respect to $k_x = 0$, the TM modes ($\psi_i = 0$) for (A) and (C) are excited and the TE modes ($\phi_i = 0$) for (B) and (D) propagate. The electric and magnetic fields in the case of (B) are expressed as

$$\begin{aligned}
 E_x &= N_i \sqrt{Z_0/R_{\{i\}}} k_y \cos k_y y \\
 E_y &= E_z = H_x = 0 \\
 H_y &= \frac{N_i}{\sqrt{Z_0/R_{\{i\}}}} k_y \cos k_y y \\
 H_z &= \frac{N_i}{\sqrt{R_{\{i\}}} Z_0} \frac{j k_y^2}{k_0} \sin k_y y.
 \end{aligned}$$

The surface impedances become $Z_{ta} = 0$, $Z_{la} = 0$ and $Z_{tb} = j(k_0/k_y) Z_0 \cot(k_y b/2)$ and $Z_{lb} = j(k_y/k_0) Z_0 \cot(k_y b/2)$. Because the separation constant is determined to be $k_y = n_o \pi/b$ with an odd number n_o from $Z_{tb} = 0$, we have $Z_{lb} = 0$. Due to $E_x = E_y = E_z = 0$, $H_x = H_y = 0$ and $H_z \neq 0$ at $y = \pm b/2$, the smooth walls at $y = \pm b/2$ can be replaced completely with the corrugated walls. Both E_x and H_y are independent of x . The profiles are different from ones of the hybrid mode with $k_x \neq 0$

Table 4: Possible wall-shape of the rectangular waveguide in the case of (D). The upper figure in the box shows the exact result and the lower one the alternative shape with the highly oversized approximation ($R_{\{i\}}^2 \simeq 1$). The absence of a figure indicates that the boundary conditions at $x = \pm a/2$ and/or $y = \pm b/2$ is not satisfied. The arrows show the main electric field.

waveguide 		$m_p(\neq 0)$					
		$d_i = -k_y/k_x$ $E_x, H_y \propto \cos k_x x \sin k_y y$ $E_y = 0, H_x \simeq 0$		$d_i = k_x/k_y$ $E_y, H_x \propto \sin k_x x \cos k_y y$ $E_x = 0, H_y \simeq 0$			
		odd	even	odd	even	odd	even
n_p ($\neq 0$)	odd						
	even						

and $k_y \neq 0$. When the square waveguide with two corrugated walls is used as an antenna, the radiation pattern cannot be kept the same for the rotation of polarization. In the case of (D), we have the TE mode property. The electric and magnetic fields are expressed as

$$\begin{aligned}
 E_x &= -N_i \sqrt{Z_0/R_{\{i\}}} k_y \sin k_y y \\
 E_y &= E_z = H_x = 0 \\
 H_y &= -\frac{N_i}{\sqrt{Z_0/R_{\{i\}}}} k_y \sin k_y y \\
 H_z &= \frac{N_i}{\sqrt{R_{\{i\}}Z_0}} \frac{jk_y^2}{k_0} \cos k_y y.
 \end{aligned}$$

The surface impedances $Z_{ta} = 0$ and $Z_{la} = 0$ are obtained, and the boundary condition $Z_{tb} = 0$ results in $k_y = n_e \pi/b$ and $Z_{lb} = 0$. Also, the electric and magnetic fields at $y = \pm b/2$ except H_z are equal to zero. The smooth walls at $y = \pm b/2$ can be replaced with corrugated walls.

With respect to $k_y = 0$, we should examine the field properties in a like manner. The two cases of (A) and (D) are valid for satisfying the boundary conditions and result in $\phi_i = 0$ which indicates a TE

mode. In the case of (A), we have

$$\begin{aligned}
 E_x &= E_z = H_y = 0 \\
 E_y &= -N_i \sqrt{Z_0/R_{\{i\}}} k_x \cos k_x x \\
 H_x &= \frac{N_i}{\sqrt{Z_0/R_{\{i\}}}} k_x \cos k_x x \\
 H_z &= \frac{N_i}{\sqrt{R_{\{i\}}Z_0}} \frac{jk_x^2}{k_0} \sin k_x x,
 \end{aligned}$$

where $k_x = m_o \pi/a$ with an odd number m_o due to $Z_{ta} = j(k_0/k_x)Z_0 \cot(k_x a/2) = 0$. The other surface impedances are $Z_{la} = j(k_x/k_0)Z_0 \cot(k_x a/2) = 0$, $Z_{tb} = 0$ and $Z_{lb} = 0$. In the case of (D), we have

$$\begin{aligned}
 E_x &= E_z = H_y = 0 \\
 E_y &= N_i \sqrt{Z_0/R_{\{i\}}} k_x \sin k_x x \\
 H_x &= -\frac{N_i}{\sqrt{Z_0/R_{\{i\}}}} k_x \sin k_x x \\
 H_z &= \frac{N_i}{\sqrt{R_{\{i\}}Z_0}} \frac{jk_x^2}{k_0} \cos k_x x,
 \end{aligned}$$

where $k_x = m_e \pi/a$ with an even number m_e due to $Z_{ta} = 0$. Thus, $Z_{la} = 0$, $Z_{tb} = 0$ and $Z_{lb} = 0$ are obtained. The smooth walls at $x = \pm a/2$ can be replaced with corrugated ones for (A) and (D) as discussed in the case of $k_x = 0$. These results on the TE mode are summarized in Table 5.

Table 5: Possible wall-shape of the rectangular waveguide with TE mode in the case of $k_x = 0$ or $k_y = 0$. The upper figure in the box shows the exact result and the lower one the alternative shape without the highly oversized approximation ($R_{\{i\}}^2 \simeq 1$). The absence of a figure indicates that the boundary conditions at $x = \pm a/2$ and/or $y = \pm b/2$ is not satisfied. The arrows show the main electric field.

	Case (A)	Case (B)	Case (C)	Case (D)
$k_x = 0$ ($m_p = 0$)		 n_p $= n_o$		 n_p $= n_e$
$k_y = 0$ ($n_p = 0$)	 m_p $= m_o$			 m_p $= m_e$

Normalization

The normalization constants N_i appearing in ψ_i and ϕ_i are determined by

$$\int \mathbf{E}_i \times \mathbf{H}_i dS = 1$$

where the integration is carried out over the entire cross-section of the waveguide. The constants N_i with $k_x \neq 0$ and $k_y \neq 0$ is

$$N_i = 2/\sqrt{ab(k_x^2 + k_y^2)(1 + d_i^2 R_{\{i\}}^2)}.$$

Also, $N_i = \sqrt{2}/(k_y \sqrt{ab})$ for $k_x = 0$ and $k_y \neq 0$ and $N_i = \sqrt{2}/(k_x \sqrt{ab})$ for $k_y = 0$ and $k_x \neq 0$ are obtained.

3 Square Corrugated Waveguide

On the label of the modes corresponding to the oversized rectangular waveguide with all the corrugated walls, the definition used in an integrated optics is suitable [11]. The (m_o, n_o) mode with $d_i = -m_o/n_o$ in (A), the (m_e, n_e) mode with $d_i = -m_e/n_e$ in (B), the (m_o, n_e) mode with $d_i = m_o/n_e$ in (C) and the (m_e, n_o) mode with $d_i = m_e/n_o$ in (D) are named as E_{mn}^y . The (m_e, n_e) mode with $d_i = n_e/m_e$ in (A), the (m_o, n_o) mode with $d_i = n_o/m_o$ in (B), the (m_e, n_o) mode with $d_i = -n_o/m_e$ in (C) and the (m_o, n_e) mode with $d_i = -n_e/m_o$ in (D) are called as E_{mn}^x . Here, the superscript indicates the direction of the main electric field in the waveguide. The electric and magnetic fields of and are summarized as

$$E_y, H_x \propto \begin{pmatrix} \sin(m_e \pi x/a) \\ \cos(m_o \pi x/a) \end{pmatrix} \begin{pmatrix} \sin(n_e \pi y/a) \\ \cos(n_o \pi y/a) \end{pmatrix}$$

with $d_i = -(-1)^{m_p+n_p} m_p/n_p$ for E_{mn}^y mode and

$$E_x, H_y \propto \begin{pmatrix} \sin(m_e \pi x/a) \\ \cos(m_o \pi x/a) \end{pmatrix} \begin{pmatrix} \sin(n_e \pi y/a) \\ \cos(n_o \pi y/a) \end{pmatrix}$$

with $d_i = (-1)^{m_p+n_p} n_p/m_p$ for E_{mn}^x mode, respectively, where, $m_e \neq 0$ and $n_e \neq 0$. As above-mentioned, there is no exact normal mode in the waveguide with all four corrugated walls. The present result from the analysis by scalar eigenfunctions of TE and TM modes is consistent with the conclusion from the impedance relation. However, it is emphasized that the two corrugated walls appear to be smooth walls due to almost no penetration of electric and magnetic fields in the corrugated gap when polarization is parallel to this wall. It is evident that two modes with mode numbers (m_p, n_p) and (n_p, m_p) in the oversized square waveguide ($a = b$) with $d = \lambda_0/4$ have the identical cutoff frequencies $k_{c\{i\}} = \sqrt{(m_p \pi/a)^2 + (n_p \pi/a)^2}$. By using the highly oversized square waveguide with all the corrugated walls, the control of the field polarization in the waveguide becomes possible. In a waveguide with two smooth and two corrugated walls which satisfies exactly the boundary condition, the cross-polarized mode on the (m_o, n_e) is the TE mode with $k_x = 0$ in (B) whose an amplitude has no x -dependence. This mode is unsuitable as polarization rotation. Meanwhile, in the square waveguide with all four corrugated walls, the E_{11}^x mode is the cross-polarized mode of E_{11}^y . Amplitude distributions of E_{11}^y and E_{11}^x modes are symmetric with respect to x - and y - axes. Both modes are suitable for an application to the polarization rotation. The E_{11}^y and E_{11}^x modes are easily obtained by the conversion from HE_{11} mode in the circular corrugated waveguide with efficiency of 99.3 % [9].

For the alternative ITER antenna for electron cyclotron heating with remote steering, the length of antenna is required to be $8a^2/\lambda_0$ (or $4a^2/\lambda_0$ for asymmetric pattern). For a beam injection larger than the critical angle into a square waveguide with all four corrugated walls, higher modes with large m_p or n_p are excited and its propagation constant $\beta_{\{i\}}$ is not close to k_0 and phase slippage occurs [5]. Because the higher modes behave as ones in the weakly oversized waveguide, the modes do not satisfy approximately the boundary condition.

4 Summary

The analysis based on two scalar eigenfunction shows that hybrid mode can exist only in the rectangular waveguide with two corrugated and two smooth walls. From the field analysis at the boundary walls, two smooth walls can be replaced with the corrugated walls if the waveguide is highly oversized. This result can explain the experimental observation in weakly and highly oversized waveguides with all four walls corrugated. The application of the highly corrugated waveguides to the remote steering system for ITER is possible for electron cyclotron heating and current drive antenna with any polarization.

Acknowledgements

The author would like to thank Drs. S. Kubo, T. Shimozuma, H. Idei and Y. Yoshimura for their discussions. He also acknowledges Drs. O. Motojima and M. Fujiwara for their continuing encouragement. This work was partially supported by Grant-in-Aid from Ministry of Education, Culture, Sports, Science and Technology.

References

- [1] M. Thumm and W. Kasperek: Fusion Engineering and Design **26**, 291, 1995.
- [2] R. B. Dybdal, R. Peters, Jr and W. H. Peake: IEEE Trans, Microwave Theory and Tech. **19**, 2, 1971.
- [3] G. H. Bryant: Proc. IEE **116**, 203, 1969.
- [4] R. Prater, H. J. Grunloh, C. P. Moeller, J. L. Doane, R. A. Olstad, M. Makowski and R. W. Harvey: Proc. 10th Workshop on ECE and ECRH, EC10, World Scientific, p531, 1997.
- [5] A. V. Chirkov, G. G. Denisov, W. Kasperek, D. Wagner, G. Gantenbein, M. Haug and F. Hollmann: Fusion Engineering and Design **53**, 465, 2001.
- [6] W. Kasperek: Private communication.
- [7] A. A. S. Obaid, T. S. M. Madean, M. Razaz: Proc. IEE **132**, 413, 1985
- [8] N. Marcuvitz: *Waveguide Handbook*, McGraw-Hill, 1951.
- [9] K. Ohkubo, S. Kubo, M. Sato, H. Idei, Y. Takita, T. Kuroda: Fusion Engineering and Design **26**, 325, 1995.
- [10] J. L. Doane: *Infrared and Millimeter Waves* edited by K. J. Button, vol. 13, Millimeter Components and Techniques, Part IV, 123, Academic Press, 1985.
- [11] D. Marcuse: *Theory of Dielectric Optical Waveguides*, p 49, Academic Press, 1974.

Recent Issues of NIFS Series

- NIFS-676 K Itoh
A Prospect at 11th International Toki Conference Plasma physics quo vadis? Jan 2001
- NIFS-677 S Satake, H Sugama, M Okamoto and M Wakatani
Classification of Particle Orbits near the Magnetic Axis in a Tokamak by Using Constants of Motion Jan 2001
- NIFS-678 M Tanaka and A Yu Grosberg,
Giant Charge Inversion of a Macroion Due to Multivalent Counterions and Monovalent Coions Molecular Dynamics Studyn Jan 2001
- NIFS-679 K Akaishi, M Nakasuga, H Suzuki, M Ima, N Suzuki, A Komori, O Motojima and Vacuum Engineering Group,
Simulation by a Diffusion Model for the Variation of Hydrogen Pressure with Time between Hydrogen Discharge Shots in LHD Feb 2001
- NIFS-680 A Yoshizawa, N Yokoi, S Nisizima, S-I Itoh and K Itoh
Variational Approach to a Turbulent Swirling Pipe Flow with the Aid of Helicity Feb 2001
- NIFS 681 Alexander A Shishkin
Estafette of Drift Resonances, Stochasticity and Control of Particle Motion in a Toroidal Magnetic Trap Feb 2001
- NIFS-682 H Momota and G H Miley,
Virtual Cathode in a Spherical Inertial Electrostatic Confinement Device Feb 2001
- NIFS-683 K Saito, R Kumazawa, T Muroh, T Seki, T Watari, Y Torii, D A Hartmann, Y Zhao, A Fukuyama, F Shimo, G Nomura, M Yokota, M Sasao, M Isobe, M Osakabe, T Ozaki, K Narihara, Y Nagayama, S Inagaki, K Itoh, S Morita, A V Krasilnikov, K Ohkubo, M Sato, S Kubo, T Shimezuma, H Idei, Y Yoshimura, O Kaneko, Y Takeiri, Y Oka, K Tsumori, K Ikeda, A Komori, H Yamada, H Funaba, K Y Watanabe, S Sakakibara, M Shoji, R Sakamoto, J Miyazawa, K Tanaka, B J Peterson, N Ashikawa, S Murakami, T Minami, S Ohakachi, S Yamamoto, S Kado, H Sasao, H Suzuki, K Kawahata, P deVries, M Emoto, H Nakanishi, T Kobuchi, N Inoue, N Ohyabu, Y Nakamura, S Masuzaki, S Muto, K Sato, T Morisaki, M Yokoyama, T Watanabe, M Goto, I Yamada, K Ida, T Tokuzawa, N Noda, S Yamaguchi, K Akaishi, A Sagara, K Toi, K Nishimura, K Yamazaki, S Sudo, Y Hamada, O Motojima, M Fujiwara,
Ion and Electron Heating in ICRF Heating Experiments on LHD Mar 2001
- NIFS-684 S Kida and S Goto,
Line Statistics Stretching Rate of Passive Lines in Turbulence Mar 2001
- NIFS-685 R Tanaka, T Nakamura and T Yabe
Exactly Conservative Semi-Lagrangian Scheme (CIP-CSL) in One-Dimension Mar 2001
- NIFS-686 S Toda and K Itoh,
Analysis of Structure and Transition of Radial Electric Field in Helical Systems Mar 2001
- NIFS-687 T Kuroda and H Sugama,
Effects of Multiple-Helicity Fields on Ion Temperature Gradient Modes Apr 2001
- NIFS-688 M Tanaka,
The Origins of Electrical Resistivity in Magnetic Reconnection. Studies by 2D and 3D Macro Particle Simulations. Apr. 2001
- NIFS-689 A Maluckov, N Nakajima, M Okamoto, S Murakami and R Kanno,
Statistical Properties of the Neoclassical Radial Diffusion in a Tokamak Equilibrium Apr 2001
- NIFS-690 Y Matsumoto, T Nagaura, Y Itoh, S-I Oikawa and T Watanabe,
LHD Type Proton-Boron Reactor and the Control of its Peripheral Potential Structure Apr 2001
- NIFS-691 A Yoshizawa, S-I Itoh, K. Itoh and N Yokoi,
Turbulence Theories and Modelling of Fluids and Plasmas Apr 2001
- NIFS-692 K Ichiguchi, T Nishimura, N Nakajima, M Okamoto, S-I Oikawa, M Itagaki,
Effects of Net Toroidal Current Profile on Mercier Criterion in Heliotron Plasma Apr 2001
- NIFS-693 W Pei, R Horuchi and T Sato,
Long Time Scale Evolution of Collisionless Driven Reconnection in a Two-Dimensional Open System: Apr. 2001
- NIFS-694 L N Vyachenslavov, K Tanaka, K Kawahata,
CO2 Laser Diagnostics for Measurements of the Plasma Density Profile and Plasma Density Fluctuations on LHD Apr 2001
- NIFS-695 T Ohkawa,
Spin Dependent Transport in Magnetically Confined Plasma May 2001
- NIFS-696 M Yokoyama, K Ida, H Sanuki, K Itoh, K Narihara, K. Tanaka, K Kawahata, N Ohyabu and LHD experimental group
Analysis of Radial Electric Field in LHD towards Improved Confinement May 2001
- NIFS-697 M Yokoyama, K. Itoh, S Okamura, K Matsuoka, S -I Itoh,
Maximum-J Capability in a Quasi-Axisymmetric Stellarator: May 2001
- NIFS-698 S-I Itoh and K Itoh,
Transition in Multiple-scale-lengths Turbulence in Plasmas May 2001
- NIFS-699 K Ohi, H Naitou, Y. Tauchi, O Fukumasa,
Bifurcation in Asymmetric Plasma Divided by a Magnetic Filter May 2001
- NIFS-700 H Miura, T Hayashi and T Sato,
Nonlinear Simulation of Resistive Ballooning Modes in Large Helical Device June 2001
- NIFS-701 G Kawahara and S Kida,
A Periodic Motion Embedded in Plane Couette Turbulence June 2001
- NIFS-702 K Ohkubo,
Hybrid Modes in a Square Corrugated Waveguide June 2001